Oral Oncology 93 (2019) 91–95

Contents lists available at ScienceDirect

Oral Oncology

journal homepage: www.elsevier.com/locate/oraloncology

Feasibility of multiparametric imaging with PET/MR in nasopharyngeal carcinoma: A pilot study

Caineng Cao[a,1], Pengfei Yang[b,c,1], Yuanfan Xu[d], Tianye Niu[b,c], Qiaoying Hu[a], Xiaozhong Chen[a,*]

[a] Department of Radiation Oncology, Zhejiang Cancer Hospital, Zhejiang Key Laboratory of Radiation Oncology, Hangzhou, Zhejiang, China
[b] Department of Radiation Oncology, Sir Run Run Shaw Hospital, Zhejiang University School of Medicine, Hangzhou, Zhejiang, China
[c] Institute of Translational Medicine, Zhejiang University, Hangzhou, Zhejiang, China
[d] Hangzhou Universal Medical Imagine Diagnostion Center, Hangzhou, Zhejiang, China

ARTICLE INFO

Keywords:
Nasopharyngeal carcinoma
PET/MR
FDG-PET
Diffusion-weighted imaging

ABSTRACT

Objective: The aim of this pilot study was to explore the integrated positron emission tomography and magnetic resonance imaging scanner (PET/MR) for biological characterization of nasopharyngeal carcinoma (NPC) and potential therapeutic applications of dose painting (DP).

Patients and methods: Twenty-one NPC patients with PET/MR were included in this study. Overlap of tumor volumes was analyzed on T2-weighted images (volume of interest, VOI_{T2}), diffusion-weighted magnetic resonance imaging (VOI_{DWI}) and ^{18}F-fluorodeoxyglucose positron emission tomography (VOI_{PET}). The overlap percentages of low-metabolic sub-region (cluster 1) and high-metabolic sub-region (cluster 2) in VOI_{PET} and VOI_{DWI} were analyzed by cluster analysis.

Results: Both the VOI_{DWI} and VOI_{PET} were encompassed in the VOI_{T2}, respectively 99.6% and 97.5%. The median tumor overlap was 94.4% (VOI_{DWI} within VOI_{PET}). The median overlap of cluster 2 in VOI_{PET} and VOI_{DWI} was 43.61% (27.67–52.66%) and 21.86%(10.47–40.89%), respectively. The median overlap of cluster 1 in VOI_{PET} and VOI_{DWI} was 48.03% (23.91–63.15%) and 24.40% (7.44–51.44%), respectively. Separation between clusters appeared to be defined by a SUV value.

Conclusion: For NPC, the VOIs of DWI and FDG PET were not overlapped completely and the volume defined by cluster-analysis might be meaningful for DP.

Introduction

Nasopharyngeal carcinoma (NPC) has a unique pattern of geographical distribution. Worldwide, 86,700 new patients with NPC were reported in 2012 with the highest incidences reported in southeast Asia [1]. Radiotherapy is the primary and only curative treatment for NPC and intensity-modulated radiotherapy (IMRT) is the preferred method to date [2]. Optimum imaging is crucial for radiotherapy planning of NPC. Magnetic resonance imaging (MRI) provides improved soft-tissue contrast and target volume delineation over computed tomography (CT) [3]. Functional MRI and ^{18}F-fluorodeoxyglucose positron emission tomography (FDG-PET) could provide additional biological information for NPC [2].

Dose painting (DP) aims at delivering a heterogeneous dose to tumors based on molecular imaging. ^{18}F-fluorodeoxyglucose positron emission tomography (FDG-PET)-guided DP-IMRT is associated with a considerable survival benefit, without increasing toxicity in NPC [4,5]. However, the reports of DP based on functional MRI are limited [6].

Integrated positron emission tomography and magnetic resonance imaging scanner (PET/MR) can provide diffusion weighted imaging (DWI) and ^{18}F-FDG uptake simultaneously, which could reduce misalignment and allow to evaluate the volume of interest (VOI) for DP. For NPC, ^{18}F–FDG PET/MR was more accurate than the combination of head and neck MRI with PET/CT in terms of tumor staging [7]. However, the feasibility of routine PET/MRI use in NPC has not yet been fully elucidated. The aim of this pilot study was to explore the integrated PET/MR for biological characterization of NPC and potential therapeutic applications of DP.

* Corresponding author at: Department of Radiation Oncology, Zhejiang Cancer Hospital, Zhejiang Key Laboratory of Radiation Oncology, No 1, East Banshan Road, Gongshu District, Hangzhou 310022, China.
E-mail address: chenxiaozhong2016@163.com (X. Chen).
[1] C.N Cao and P.F Yang contributed equally to this work.

https://doi.org/10.1016/j.oraloncology.2019.04.021
Received 5 March 2019; Received in revised form 6 April 2019; Accepted 27 April 2019
Available online 01 May 2019
1368-8375/

Material and methods

Patients

Between May 2017 and January 2018, 22 histologically confirmed NPC patients underwent PET/MR for tumour staging. Of the 22 patients, 1 was excluded from this study for signal drop out on DWI (Supplemental Fig. 1). All patients were asked to fast for at least 6 h before undergoing PET/MR examination. Each subject was scanned under the imaging protocol which consisted of injecting 18F-FDG (3.7 MBq/kg) and starting the scan after approximately 2 h of uptake.

Supplementary data associated with this article can be found, in the online version, at https://doi.org/10.1016/j.oraloncology.2019.04.021.

Whole-body ^{18}F-FDG PET/MR

PET/MRI was performed on a SIGNA PET/MR (GE Healthcare). The PET/MRI system was equipped with a 3-T magnetic field strength, total imaging matrix coil technology covering the entire body with multiple integrated radiofrequency surface coils, and a fully functional PET system with silicon photomultiplier (SiMP) embedded in the magnetic resonance gantry.The PET scanner had a reported spatial resolution of 4.66 mm full width at half maximum (FWHM) at 1 cm, and 5.23 mm FWHM at 10 cm from the transverse field-of-view (FOV), and a sensitivity of 22.9 kcps/MBq at the center of the FOV. The examination protocol combined a whole-body scan with a dedicated examination of the head and neck area.

After performing the sequence for attenuation correction, a whole-body PET scan was conducted from the head to the hip (craniocaudal) in five bed positions, with an acquisition time of 6 min per bed position. During PET data acquisition, whole-body MRI was performed. Subsequently, regional PET and MRI were simultaneously performed. Regional PET was performed with an acquisition time of 10 min, while dedicated MRI coil of the head and neck region was acquired to get the axial, coronal and sagittal images (Table 1). The PET data were reconstructed using ordered subset expectation maximum (OSEM) with time-of-flight (TOF) information reconstruction and point spread function (PSF) correction, with three iterations, 28 subsets, and a 4-mm Gaussian post processing filter, into 192 × 192 matrices.

Volume of interest

The VOI for the primary tumor was defined on T2-weighted images (VOI_{T2}), DWI (VOI_{DWI}) and PET (VOI_{PET}), respectively. Without access to or evaluation of the PET and DWI images, the VOI_{T2} was delineated.

Table 1
MRI sequence parameters used for integrated PET/MRI.

Region	Sequence	TR	TE	ST	FOV	T
Whole body	Ax LAVA-Flex T1	4.4	2.4	4.8	440	1:15
Whole body	Ax FRFSE T2	4000	86.3	8.0	440	11:00
Whole body	Sag T2SSFSE	1302	67.7	5.0	480	1:09
Whole body	Ax DWI (b-values: 0.800 s/mm^2)	11,250	59.9	8.0	440	9:50
Head Neck	Sag T2 FSE	2674	88.5	4	280	3:24
Head Neck	Cor T1 FSE	629	12.1	4	280	3:17
Head Neck	Cor T2 IDeal	4612	66.9	4	280	5:18
Head Neck	Ax T1 FSE	693	11.4	4	220	2:38
Head Neck	Ax T2 IDeal	4404	66	4	220	4:38
Head Neck	Ax DWI (b-values: 0.1000 s/mm^2)	4621	63.6	4	220	3:14

Abbreviations: TR repetition time in ms, TE echo time in ms, ST Slice thickness in mm, FOV field of view in mm, T scanning time in min, FRFSE fast recovery fast spin echo, DWI diffusion weighted imaging, SSFSE single-shot fast spin echo, FSE fast spin echo.

The VOIPET was defined as SUV iso-contour starting at 40% of the SUVmax [8].

Analysis of DWI and PET data

The volume metrics of overlap between VOIs defined on T2-MRI, DWI-MRI and PET were calculated using in-house developed software implanted in MATLAB 2017b (MathWorks, Natick, MA). Tumor volume overlap between the respective imaging modalities was assessed as a percent-wise overlap.

To investigate a potential association between SUV and ADC values of NPC, an ADC map was generated by the scanner software AW4.6 (GE Healthcare, USA) using two b-values (b-0, b-1000 s/mm^2). After automatic transfer on the corresponding parameter map and visual confirmation of a correct placement, ADC values were determined. The correlation between SUV and ADC was assessed at patient level. The maximum value of SUV, minimum value of ADC and mean value of SUV and ADC were used in the correlation analysis.

A voxel-wise analysis of correlation between SUV and ADC was also executed in this study using MATLAB 2017b. All voxels present in the overlapped VOIs (PET and DWI) were used in the voxel-wise analysis. The K-means method was used to perform tumor clustering based on the ADC map and SUV map. The K-means method partition the tumor region into 2 clusters [9], where each voxel in the tumor region belongs to the cluster with the nearest mean. The K-means method has been used in liver cancer [10], lung cancer [11] for partitioning tumor sub-regions and showed promising results. In this study, the cluster region with lower SUV was defined as Cluster 1 and the region with higher SUV was defined as Cluster 2. The volume of tumor sub-region with higher SUV which were more metabolically active was reported to be predictive of overall survival and out-of-field progression in lung cancer [9]. So the overlap percentages of low-metabolic sub-region (cluster 1) and high-metabolic sub-region (cluster 2) in VOI_{PET} and VOI_{DWI} were also calculated in this study.

Statistical analysis

Statistical analysis was performed in SPSS version 19. Mann-Whitney U tests were used for the comparison of VOI_{DWI} and VOI_{PET}. Pearson correlation analysis and Spearmańs rank correlation was used for the correlations of ADC and SUV.

Results

Baseline characteristics

There were 15 male patients and 6 female patients, with a male to female ratio of 2.5:1.0. The median age was 51 years (range, 28–77 years). Histologically, all patients had non-keratinizing carcinoma. According to the 8th AJCC (American joint committee on Cancer) staging system, the stage distribution for all patients was 4.8% Stage II (n = 1), 33.3% Stage III (n = 7), 52.4% Stage IVA (n = 11), and 9.5% Stage IVB (n = 2).

Overlap of tumor volumes

The volumes from the three imaging modalities are illustrated in Fig. 1. The VOI_{PET} yielded values smaller than the VOI_{DWI} ($p = 0.007$). The median VOI of DWI, FDG PET and T2-weighted images and the tumor overlap between each modality are shown in Table 2. Both the VOI_{DWI} (99.6%) and VOI_{PET} (97.5%) were encompassed in the VOI_{T2}, respectively. In all but 1 patient, more than 66% of the VOI_{DWI} was encompassed in VOI_{PET}. In the remaining patient, only 58.4% of VOI_{DWI} was encompassed in VOI_{PET}. The median tumor overlap was 94.4% (VOI_{DWI} within VOI_{PET}) (Table 2). Two examples of mismatch of VOI_{PET} and VOI_{DWI} are shown in Fig. 2.

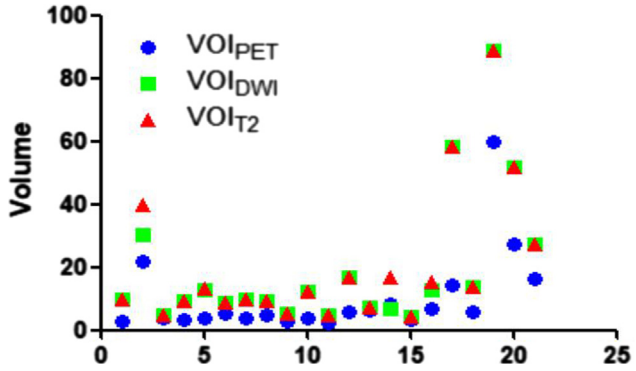

Fig. 1. Tumor volumes measured with diffusion weighted imaging (VOI_{DWI}), PET imaging (VOI_{PET}) and with anatomical T2 imaging (VOI_{T2}) on PET/MR.

Table 2
The VOI of DWI, FDG PET and T2-weighted images and the tumor overlap between each modality.

	Median (range)
VOI_{PET} (cc)	5.4(2.2–59.9)
VOI_{DWI} (cc)	9.9(4.1–88.8)
VOI_{T2} (cc)	12.3(4.1–88.8)
VOI_{PET} in VOI_{DWI} (%)	46.1(18.2–90.4)
VOI_{DWI} in VOI_{PET} (%)	94.4(58.4–100.0)
VOI_{DWI} in VOI_{T2} (%)	99.6(59.3–100.0)
VOI_{PET} in VOI_{T2} (%)	97.5(74.0–100.0)

Abbreviations: VOI Volume of interest, DWI diffusion-weighted magnetic resonance imaging, FDG PET ^{18}F-fluorodeoxyglucose positron emission tomography.

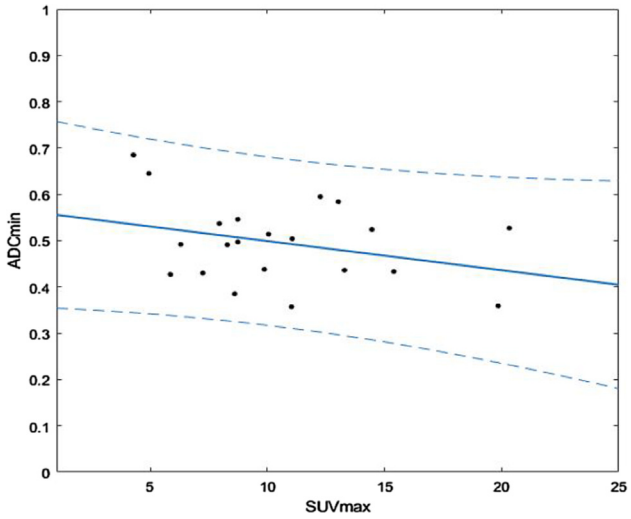

Fig. 3. Scatterplot of SUVmax and ADCmin. The data is fitted to a linear model, and layed over with a 95% confidence-interval (blue). (For interpretation of the references to colour in this figure legend, the reader is referred to the web version of this article.)

between SUV and ADC was observed in 42 of 60 axial images with mean correlation coefficient of −0.261 (range −0.732; 0.327).

Cluster analysis

The median overlap of cluster 2 in VOI_{PET} and VOI_{DWI} was 43.61% (27.67–52.66%) and 21.86% (10.47–40.89%), respectively. The median overlap of cluster 1 in VOI_{PET} and VOI_{DWI} was 48.03% (23.91–63.15%) and 24.40% (7.44–51.44%), respectively. Separation between clusters appeared to be defined by a SUV value (Supplemental Fig. 2). The cluster analysis of the 'representative overlap' patient and the 'poor overlap' patient using axial images from the DWI and PET scans are shown in Fig. 4.

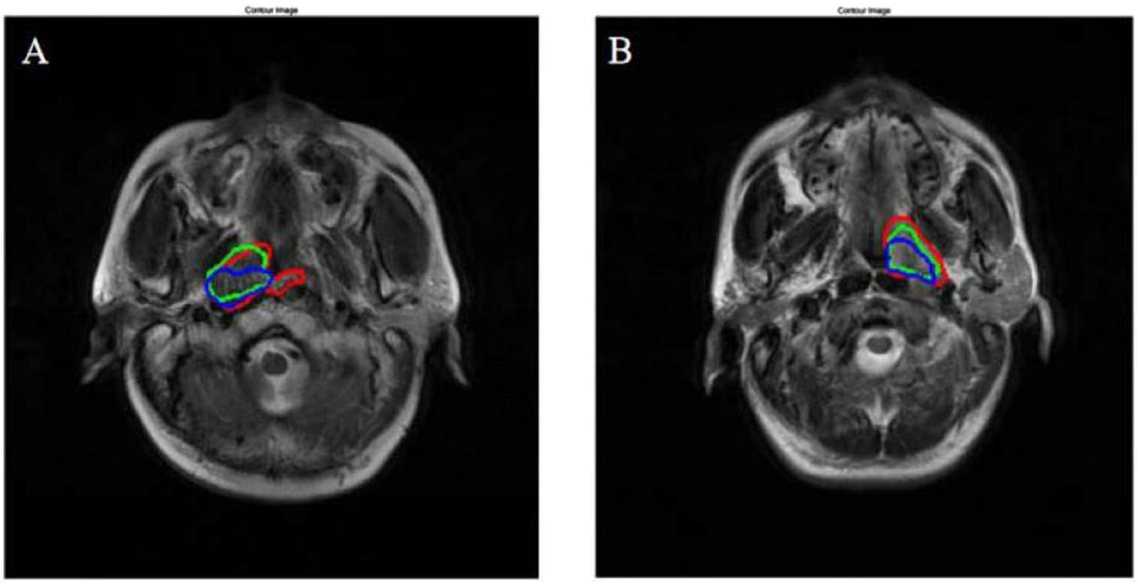

Fig. 2. Examples of tumor overlap between tumor defined from diffusion weighted imaging (green contour), tumor defined from FDG PET/MR (blue contour) and T2 weighted MR (red contour). A worst case (A) and a representative case (B). (For interpretation of the references to colour in this figure legend, the reader is referred to the web version of this article.)

ADC and SUV

A scatter plot of ADC_{min} and SUV_{max} is shown in Fig. 3. No significant difference between ADC_{min} and SUV_{max} was observed with correlation coefficients of −0.316 ($p = 0.164$). Similarly, no significant difference between ADC_{mean} and SUV_{mean} was observed with correlation coefficients of −0.326 ($p = 0.149$). On a voxel-wise level, a total of 60 axial images were evaluated. Significantly negative correlation

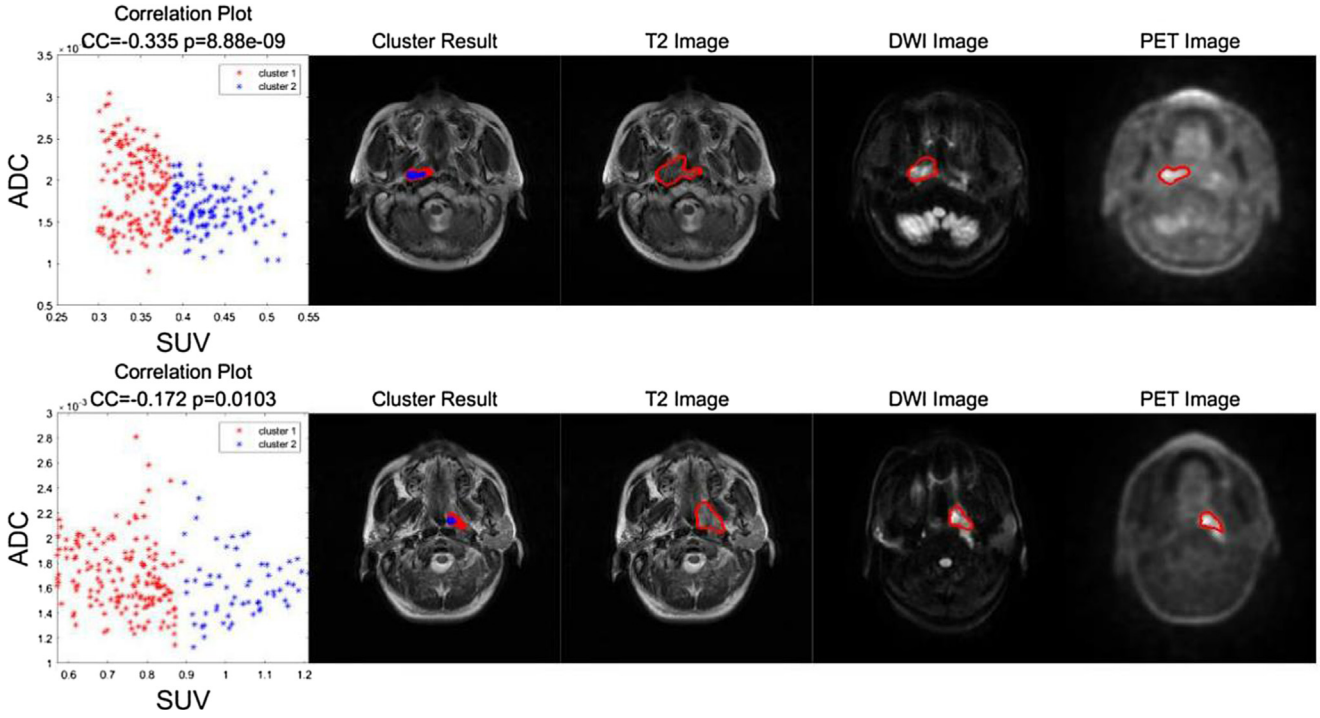

Fig. 4. The voxel-by-voxel analysis showing the respective clustering assignment from the cluster analysis for the patient in Fig. 2A, B.

Discussion

The tumor overlap between VOI_{PET} and VOI_{DWI} was not complete. More than 90% of VOI_{DWI} was encompassed in VOI_{PET} and nearly half (46.1%) of VOI_{PET} was encompassed in VOI_{DWI}. No significant correlation between SUV and ADC was observed in terms of the quantifiable measures (SUV_{max} and ADC_{min}, SUV_{mean} and ADC_{mean}). However, the correlation was significant on a voxel-wise level. The cluster analysis was feasible and identified a volume encompassing nearly half of VOI_{PET}.

With the benefit of treatment individualization and sparing of organs at risk, FDG-PET is increasingly used in NPC for DP [6,12,13]. Various threshold methods such as SUV2.5, SUV50%max, and signal/background ratio have been adopt for DP [5,6,14–16]. In the study of investigating the correlation of PET/MR in head and neck cancer, SUV40%max was adopt to define the VOI_{PET} for including the SUV-avid tissue and excluding physiological uptake [9]. In the study of tumor delineation using 18F-FDG PET/CT for NPC, SUV40%max indicated higher similarity with VOI based on MRI than SUV50%max [17]. Since no consensus has been acheived in DP to define target for NPC, SUV40%max is adopt in this study.

FDG-PET-guided DP-IMRT is associated with a considerable survival benefit for NPC [5]. In the study of exploring the feasibility of ^{18}F-Fluorothymidine (^{18}F-FLT) PET in predicting treatment response of NPC, 20 patients with NPC of Stage II-IVB were enrolled and preliminary results showed both ^{18}F-FLT PET had the potential to monitor and predict tumor regression [18]. The substitution of other PET tracers such as ^{18}F-FLT, urokinase-type plasminogen activator receptor for FDG could provide valuable additional information for precision medicine [18–20], which might be useful for improving therapy planning and treatment monitoring.

The overlap of VOI_{DWI} and VOI_{PET} for NPC is not complete in the present study. The partial overlap demonstrated in this study is in concordance with the previous studies of head-and-neck cancer [6,9]. Since ADC and SUV were proven to be prognostic factors of NPC [21,22], the volume defined by cluster-analysis such as the volume of SUVmax and ADCmin might be meaningful for DP, which needs to be confirmed in histological correlation or failure pattern analysis [23]. The present results indicat that DWI-MRI and FDG-PET provide complementary information. It is possible to deduce the information of FDG-PET from DWI-MRI with machine learning approaches in the future [24], which is meaningful for patients receiving non-FDG for PET/MR imaging. Moreover, multiparametric MRI-based radiomics from primary tumor provided improved prognostic ability in NPC [25]. The PET/MR radiomics based clinical trial of NPC (NCT03657017) is ongoing in our center. Artificial intelligence in PET/MRI of NPC should be elucidated in the future [26].

In the present study, no significant correlation between SUV and ADC was observed in terms of the quantifiable measures and significant correlation was observed on a voxel-wise level, which was similar to the studies of head and neck cancer with PET/MR [6,9]. It indicates that information on ADC and SUV from only one voxel is not enough to access the potential correlation. With the development of radiomics in NPC [25], it is reasonable to evaluate the correlation between SUV and ADC on a voxel-wise level. Of note, the determination of ADC and SUV correlations may be affected by other factors, such as geometrical distortions [27]. Geometrical distortions are particularly present in the ADC maps (Supplemental Fig. 1). Ideally MRI sequences and new methods for geometrical distortion correction are needed [28,29].

Conclusion

For NPC, the VOIs of DWI and FDG PET were not overlapped completely and the volume defined by cluster-analysis might be meaningful for DP.

Funding

This work was supported by a grant from the Natural Science Foundation of Zhejiang Province (No. LGF19H160007).

Conflicts of interest

None declared.

References

[1] Torre LA, Bray F, Siegel RL, Ferlay J, Lortet-Tieulent J, Jemal A. Global cancer statistics, 2012. CA Cancer J Clin 2015;65:87–108.
[2] Chua ML, Wee JT, Hui EP, Chan AT. Nasopharyngeal carcinoma. Lancet 2016;387(10022):1012–24.
[3] Chin AL, Lin A, Anamalayil S, Teo BK. Feasibility and limitations of bulk density assignment in MRI for head and neck IMRT treatment planning. J Appl Clin Med Phys 2014;15(5):4851.
[4] Ling CC, Humm J, Larson S, Amols H, Fuks Z, Leibel S, et al. Towards multi-dimensional radiotherapy (MD-CRT): Biological imaging and biological conformality. Int J Radiat Oncol Biol Phys 2000;47:551–60.
[5] Liu F, Xi XP, Wang H, Han YQ, Xiao F, Hu Y, et al. PET/CT-guided dose-painting versus CT-based intensity modulated radiation therapy in locoregional advanced nasopharyngeal carcinoma. Radiat Oncol 2017;12(1):15.
[6] Houweling AC, Wolf AL, Vogel WV, Hamming-Vrieze O, van Vliet-Vroegindeweij C, van de Kamer JB, et al. FDG-PET and diffusion-weighted MRI in head-and-neck cancer patients: implications for dose painting. Radiother Oncol 2013;106:250–4.
[7] Chan SC, Yeh CH, Yen TC, Ng SH, Chang JT, Lin CY, et al. Clinical utility of simultaneous whole-body 18F-FDG PET/MRI as a single-step imaging modality in the staging of primary nasopharyngeal carcinoma. Eur J Nucl Med Mol Imaging 2018;45(8):1297–308.
[8] Bayne M, Hicks RJ, Everitt S, Fimmell N, Ball D, Reynolds J, et al. Reproducibility of "intelligent" contouring of gross tumor volume in non-small-cell lung cancer on PET/CT images using a standardized visual method. Int J Radiat Oncol Biol Phys 2010;77:1151–7.
[9] Rasmussen JH, Nørgaard M, Hansen AE, Vogelius IR, Aznar MC, Johannesen HH, et al. Feasibility of multiparametric imaging with PET/MR in head and neck squamous cell carcinoma. J Nucl Med 2017;58(1):69–74.
[10] Xia W, Chen Y, Zhang R, Yan Z, Zhou X, Zhang B, et al. Radiogenomics of hepatocellular carcinoma: multiregion analysis-based identification of prognostic imaging biomarkers by integrating gene data-a preliminary study. Phys Med Biol 2018;63(3):035044.
[11] Wu J, Gensheimer MF, Dong X, Rubin DL, Napel S, Diehn M, et al. Robust intratumor partitioning to identify high-risk subregions in lung cancer: a pilot study. Int J Radiat Oncol Biol Phys 2016;95(5):1504–12.
[12] Berwouts D, Olteanu LA, Duprez F, Vercauteren T, De Gersem W, De Neve W, et al. Three-phase adaptive dose-painting-by-numbers for head-and-neck cancer: initial results of the phase I clinical trial. Radiother Oncol 2013;107(3):310–6.
[13] Olteanu LA, Madani I, De Neve W, Vercauteren T, De Gersem W. Evaluation of deformable image coregistration in adaptive dose painting by numbers for head-and-neck cancer. Int J Radiat Oncol Biol Phys 2012;83(2):696–703.
[14] Wang J, Zheng J, Tang T, Zhu F, Yao Y, Xu J, et al. A randomized pilot trial comparing Position Emission Tomography (PET)-guided dose escalation radiotherapy to conventional radiotherapy in chemoradiotherapy treatment of locally advanced nasopharyngeal carcinoma. PLoS ONE 2015;10(4):e0124018.
[15] Rasmussen JH, Håkansson K, Vogelius IR, Aznar MC, Fischer BM, Friborg J, et al. Phase I trial of 18F-Fludeoxyglucose based radiation dose painting with concomitant cisplatin in head and neck cancer. Radiother Oncol 2016;120(1):76–80.
[16] Differding S, Sterpin E, Janssens G, Hanin FX, Lee JA, Grégoire V. Methodology for adaptive and robust FDG-PET escalated dose painting by numbers in head and neck tumors. Acta Oncol 2016;55(2):217–25.
[17] Chen YZ, Li WF, Wang JY, Wang JM, Ou RY, Zheng XW, et al. Evaluation of time-phase effect on 18F-FDG PET/CT delineation methods for treatment planning of nasopharyngeal carcinoma. Clin Nucl Med 2016;41(5):354–61.
[18] Qi S, Zhongyi Y, Yingjian Z, Chaosu H. 18F-FLT and 18F-FDG PET/CT in predicting response to chemoradiotherapy in nasopharyngeal carcinoma: preliminary results. Sci Rep 2017;7:40552.
[19] Bailey DL, Antoch G, Bartenstein P, Barthel H, Beer AJ, Bisdas S, et al. Combined PET/MR: The real work has just started. Summary report of the third international workshop on PET/MR imaging. Mol Imaging Biol 2015:25672749.
[20] Persson M, Skovgaard D, Brandt-Larsen M, Christensen C, Madsen J, Nielsen CH, et al. First-in-human uPAR PET: Imaging of cancer aggressiveness. Theranostics 2015;5:1303–16.
[21] Yan DF, Zhang WB, Ke SB, Zhao F, Yan SX, Wang QD, et al. The prognostic value of pretreatment tumor apparent diffusion coefficient values in nasopharyngeal carcinoma. BMC Cancer 2017;17(1):678.
[22] Huang Y, Feng M, He Q, Yin J, Xu P, Jiang Q, et al. Prognostic value of pretreatment 18F-FDG PET-CT for nasopharyngeal carcinoma patients. Medicine (Baltimore) 2017;96(17):e6721.
[23] Due AK, Vogelius IR, Aznar MC, Bentzen SM, Berthelsen AK, Korreman SS, et al. Recurrences after intensity modulated radiotherapy for head and neck squamous cell carcinoma more likely to originate from regions with high baseline [18F]-FDG uptake. Radiother Oncol 2014;111:360–5.
[24] Ozer S, Langer DL, Liu X, Haider MA, van der Kwast TH, Evans AJ, et al. Supervised and unsupervised methods for prostate cancer segmentation with multispectral MRI. Med Phys 2010;37(4):1873–83.
[25] Zhang B, Tian J, Dong D, Gu D, Dong Y, Zhang L, et al. Radiomics features of multiparametric MRI as novel prognostic factors in advanced nasopharyngeal carcinoma. Clin Cancer Res 2017;23(15):4259–69.
[26] Bi WL, Hosny A, Schabath MB, Giger ML, Birkbak NJ, Mehrtash A. Artificial intelligence in cancer imaging: clinical challenges and applications. CA Cancer J Clin. 2019;69(2):127–57.
[27] Leibfarth S, Simoncic U, Mönnich D, Welz S, Schmidt H, Schwenzer N, et al. Analysis of pairwise correlations in multi-parametric PET/MR data for biological tumor characterization and treatment individualization strategies. Eur J Nucl Med Mol Imaging 2016;43:1199–208.
[28] Koyasu S, Iima M, Umeoka S, Morisawa N, Porter DA, Ito J, et al. The clinical utility of reduced-distortion readoutsegmented echo-planar imaging in the head and neck region: initial experience. Eur Radiol 2014;24(12):3088–96.
[29] Windischberger C, Robinson S, Rauscher A, Barth M, Moser E. Robust field map generation using a triple-echo acquisition. J Magn Reson Imaging 2004;20(4):730–4.